Sulphate partitioning into calcite: Experimental verification of pH control and application to seasonality in speleothems

Peter M. Wynn [a,*], Ian J. Fairchild [b], Andrea Borsato [c], Christoph Spötl [d],
Adam Hartland [e], Andy Baker [f], Silvia Frisia [c], James U.L. Baldini [g]

[a] Lancaster Environment Centre, University of Lancaster, Lancaster LA1 4YQ, UK
[b] School of Geography, Earth and Environmental Sciences, University of Birmingham, Birmingham, Edgbaston B15 2TT, UK
[c] School of Environmental and Life Sciences, The University of Newcastle, Callaghan, NSW 2308, Australia
[d] Institut für Geologie, Leopold-Franzens-Universität Innsbruck, Innrain 52, 6020 Innsbruck, Austria
[e] Environmental Research Institute, Science and Engineering, University of Waikato, Hamilton 3240, New Zealand
[f] Connected Waters Initiative Research Centre, UNSW Sydney, Sydney, NSW 2052, Australia
[g] Department of Earth Sciences, University of Durham, Durham DH1 3LE, UK

Abstract

Carbonate-associated sulphate (CAS) is a useful carrier of palaeoenvironmental information throughout the geologic record, particularly through its stable isotope composition. However, a paucity of experimental data restricts quantitative understanding of sulphate incorporation into carbonates, and consequently CAS concentrations and their diagenetic modifications are rarely interpreted. However, in the case of calcite speleothems, the remarkably high-resolution CAS records which are obtainable via modern microanalytical techniques represent a potentially invaluable source of palaeoenvironmental information. Here, we describe the results of controlled experiments of sulphate co-precipitation with calcite in freshwater solutions where pH, saturation state, and sulphate concentration were varied independently of each other. Solution pH is confirmed as the principal control on sulphate incorporation into calcite. The relative efficiency of incorporation was calculated as a partition coefficient $D_{SO_4} = (mSO_4/mCO_3)_{solid}/(mSO_4/mCO_3)_{solution}$. High crystal growth rates (driven by either pH or saturation state) encouraged higher values of D_{SO_4} because of an increasing concentration of defect sites on crystal surfaces. At low growth rates, D_{SO_4} was reduced due to an inferred competition between sulphate and bicarbonate at the calcite surface. These experimental results are applied to understand the incorporation of sulphate into speleothem calcite. The experimentally determined pH-dependence suggests that strong seasonal variations in cave air PCO_2 could account for annual cycles in sulphate concentration observed in stalagmites. Our new experimentally determined values of D_{SO_4} were compared with D_{SO_4} values calculated from speleothem-drip water monitoring from two caves within the Austrian and Italian Alps. At Obir cave, Austria, D_{SO_4} ($\times 10^5$) varies between 11.1 (winter) and 9.0 (summer) and the corresponding figures for Ernesto cave, Italy, are 15.4 (winter) and 14.9 (summer). These values approximate predicted D_{SO_4} values based on our chamber experiments containing both low (2 ppm) and high (20 ppm) sulphate concentrations. Our experimental values of D_{SO_4} obtained at crystal growth rates typical of stalagmites, closely match those observed in other cave sites from around the world. This validates the universality of the controls behind D_{SO_4} and will enhance the use of speleothem CAS as a palaeoenvironmental proxy.
© 2018 The Authors. Published by Elsevier Ltd. This is an open access article under the CC BY license (http://creativecommons.org/licenses/by/4.0/).

Keywords: Carbonate Associated Sulphate; Speleothem; Partition Coefficient; Sulphate; pH

---

* Corresponding author.
  E-mail address: p.wynn@lancaster.ac.uk (P.M. Wynn).

1. INTRODUCTION

Carbonate-associated sulphate (CAS) has long been recognized as a tool for understanding past environmental processes (Burdett et al., 1989). Most literature focuses on its isotope composition in marine archives as being indicative of global processes affecting sulphur cycling (e.g. Bottrell and Newton, 2006; Rennie and Turchyn, 2014). Sulphur and oxygen isotope systematics of CAS have also been used in marine and freshwater environments to inform on regimes of high atmospheric PCO_2 in ancient time (Bao et al., 2008, 2009; Benn et al., 2015) and for more recent environments, sulphur isotope systematics of CAS in speleothems has been used to reconstruct loading of SO_2 emissions to the atmosphere (Wynn et al., 2008, 2010). However, in contrast to isotopic studies, interpretations based purely on CAS concentrations are more limited due to uncertainty surrounding the nature of sulphate incorporation into the carbonate lattice. Even though lattice-substitution of analogue ion SeO_4^{2-} has been demonstrated by Reeder et al. (1994) and substitution of carbonate by sulphate was directly demonstrated by the X-ray absorption studies of Pingitore et al. (1995), the lack of a quantitative understanding of sulphate incorporation into carbonates currently limits interpretation.

The only experimental study on CAS incorporation was carried out by Busenberg and Plummer (1985) for marine-analogue systems. They interpreted results using a thermodynamic model in which a Berthelot-Nernst distribution coefficient (McIntyre, 1963) was defined as:

$$D_{SO_4} = (SO_4/CO_3)_{calcite}/(SO_4/CO_3)_{solution} \qquad (1)$$

This implied that sulphate incorporation was facilitated at lower pH where the ratio of aqueous CO_3^{2-}/HCO_3^- is lower. However, at the high ionic strength, fast growth rates and high absolute SO_4 concentrations of these experiments (100–10,000 ppm SO_4 in growth media), kinetic factors also influenced the system, and there was a strong correlation between the value of D_{SO_4} and precipitation rate. When applied to a typical speleothem-forming site (Frisia et al., 2005), these experimental results under-predicted S abundance in speleothem calcite by an order of magnitude. This mismatch was the impetus for the current study to derive experimental data representative of freshwater environments.

The sulphate content of speleothem carbonate has recently become appreciated as a valuable record of the changing sulphur biogeochemical cycle at a local to regional scale. Where atmospheric sulphur is deposited through precipitation, and cycling of sulphur through the biomass above the cave can be accounted for, secular trends in speleothem sulphur content can record regional pollution characteristics (Frisia et al., 2005; Wynn et al., 2008, 2010; Uchida et al., 2013), as well as infer volcanic events (Frisia et al., 2008; Badertscher et al., 2014) and periods of biomass burning (Nagra et al., 2016; Treble et al., 2016). However, beyond the long-term trends in speleothem sulphur content, there is much information still to be revealed by addressing sulphur dynamics at the sub-annual scale. When analysing speleothem sulphate content at high resolution, a clear high-resolution cyclicity is revealed despite minimal short-term variation in the sulphate content of the associated drip waters (Frisia et al., 2005; Fairchild et al., 2010; Wynn et al., 2014). The driver behind such high-resolution speleothem sulphate dynamics must therefore be associated with processes of sulphate incorporation during carbonate precipitation and speleothem growth.

It is well established that seasonal variation in PCO_2 of cave air has a direct effect on the rate of speleothem carbonate deposition. In most temperate caves, strong density-driven winter air circulation lowers cave air PCO_2 (Fairchild and Baker, 2012; James et al., 2015). These conditions will promote drip water degassing, consequently increasing drip water pH and calcite saturation state. Cave air PCO_2 therefore drives variability in drip water carbonate content and (in the absence of strong changes in drip rate) speleothem growth rate within an annual cycle. Following the arguments of Busenberg and Plummer (1985), a pH-driven variation in CAS incorporation should occur such that sulphate incorporation is dependent upon the ratio to carbonate ions in solution. If cave air PCO_2 varies seasonally, this should give rise to cyclicity in speleothem sulphate content with low winter and high summer concentrations which are independent of cave drip water sulphate content. Independent markers of seasonality in some caves are provided by annual flushes of fluorescent organic matter with associated colloids (Baker et al., 2008; Fairchild and Baker, 2012). Using such markers, seasonal SO_4 cycles (a winter trough and a summer peak) in speleothems from two Alpine caves have been found to be in qualitative agreement with changes in cave air PCO_2 (Fairchild et al., 2010; Wynn et al., 2014) (Fig. 1).

To test this theory of sulphate incorporation into speleothem calcite, we use our experimental set-up to simulate the partitioning of sulphate between aqueous media and carbonate deposits under conditions appropriate to dilute cave waters, such as has been carried out on other species (Huang and Fairchild, 2001; Day and Henderson, 2013). A novel feature of the experimental design is the ability to control calcite supersaturation and pH independently, in order to distinguish these as controlling variables. We also use two different sulphate concentrations covering the range typically found in cave drip waters. Experimental results are compared to two European Alpine caves: Obir Cave (Spötl et al., 2005; Fairchild et al., 2010), Austria; and Grotta di Ernesto (Frisia et al., 2005; Borsato et al., 2007; Wynn et al., 2010, 2013), Italy, where sample analysis at high temporal resolution demonstrates the seasonality of sulphate partitioning between cave waters and speleothem calcite. Summary data from other globally-distributed cave sites also allow calculation of partition co-efficients between sulphur contained in drip waters and speleothem calcite, albeit at a lower temporal resolution. In all cave sites, values of in-cave D_{SO_4} are close to the experimental data, which suggests a universal set of controls on the efficiency of sulphate incorporation into speleothem calcite, governed primarily by pH, aqueous sulphate concentration and growth rate.
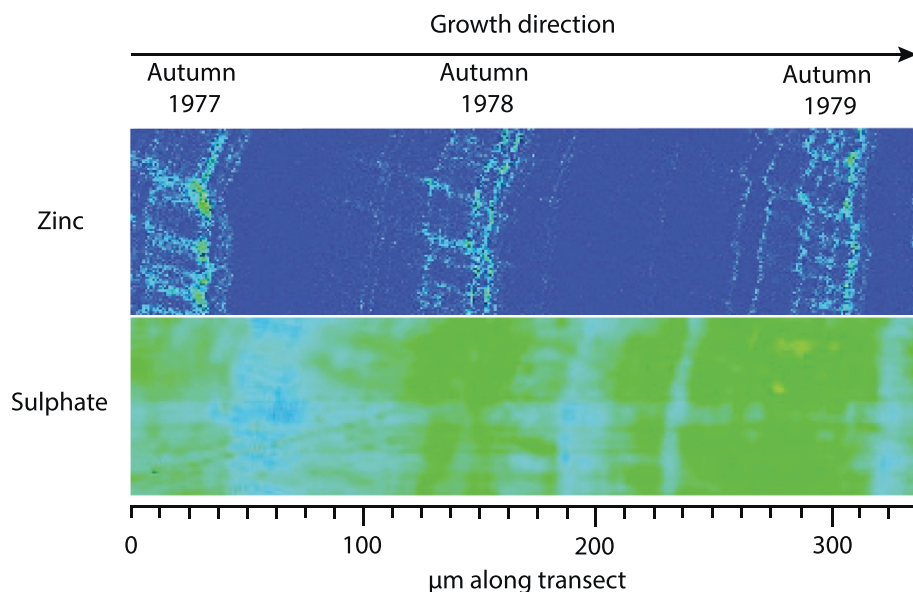
Fig. 1. Micro X-ray fluorescence mapping of speleothem sulphate and zinc content in sample Obi84. Concentrations are relative and denoted according to colour temperature scale with deep blue representing the lowest and yellow the highest concentrations in both sulphate and zinc maps. Autumnal peaks in colloidally transported elements (shown here as a Zn trace) are clearly demarcated, allowing attribution of summer high and winter low concentrations of sulphur within an annual cycle. In contrast to the clear pulses of colloidal elements recorded within the speleothem calcite, the sulphate content poorly defines the seasonal switch in ventilation regime which should cause a rapid change in drip water pH and sulphate incorporation. Figure adapted from Wynn et al. (2014).

2. METHODOLOGY

2.1. Carbonate crystal growth experiments

A simple experimental design was adopted in which solutions of defined calcite supersaturation were seeded with calcite crystals. Solutions were left to precipitate, with the aim of producing a fairly constant rate of growth for each experiment, within the range of growth equating to typical rates of linear extension for stalagmites (20–1000 μm/year) (McDermott et al., 1999).

Experiments were designed to cover a range of calcite saturation states and pH (Fig. 2 and Fig. S1). Multiple experiments were carried out simultaneously in gas-tight Pyrex© bottles of either 1 L or 0.5 L volume with a head-space of 120 ml. The existence of a headspace helps maintain supersaturation by permitting degassing of carbon dioxide. Following Henry's Law, the maximum moles of CO_2 degassed are calculated to be only 3% of total moles of $CaCO_3$ precipitated as most of the CO_2 generated remains in solution. Growth media were prepared from a mixed stock solution to produce different solution concentrations containing $CaCl_2$ and $NaHCO_3$ as follows: C1N1 = $CaCl_2$ (3.5 mM) and $NaHCO_3$ (7 mM); C05N05 = $CaCl_2$ (1.75 mM) and $NaHCO_3$ (3.5 mM); and C1.5N1.5 = $CaCl_2$ (5.25 mM) and $NaHCO_3$ (10.5 mM). The pH of each starting solution was then adjusted by addition of HCl or NaOH to achieve the compositions shown in Fig. 2 (equivalent PCO_2 values are shown in Fig. S1). Seed crystals of calcite were grown from a solution of 0.8 M $NaHCO_3$ and 0.4 M $CaCl_2$ resulting in rhombic crystals
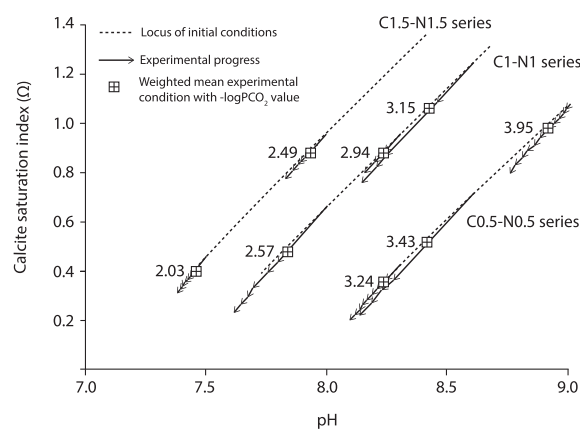

Fig. 2. Experimental conditions of pH and calcite saturation for each growth chamber depicting conditions prior to calcite precipitation and throughout the experiment duration. The weighted mean conditions of each experiment are plotted, and dashed lines represent the locus of possible original experimental conditions based on growth media composition. The calcite saturation index (Ω) is calculated as Ω = log ionic activity product over solubility product.

ca. 18 μm diameter, with specific surface area of 0.15 m²/g. Each experiment was doped with sulphate (as sodium sulphate solution) to produce a final growth media concentration of either 2 mg/L (0.02 mM) (low-sulphate experiments) or 20 mg/L (0.2 mM) (high-sulphate experiments). See Table 1 for the full range of experimental conditions.

After preparation of growth media, addition of seed crystals and adjustment of pH to the desired starting value,

chambers were left to precipitate $CaCO_3$. During the process of calcium carbonate precipitation, electrical conductivity (EC) declined due to the removal of calcium and carbonate ions from solution, and pH was lowered by the production of CO_2. EC was measured using a Tetracon 325 conductivity probe and WTW 340i combination meter, ref 25 °C. pH was monitored using a Hamilton Liq-glass™ electrode and WTW 340i meter automatically compensated to a reference temperature of 25 °C and calibrated to buffer solutions of pH 4.0 and 7.01 on use (precision ± 0.01 pH units within two units from the calibration point). pH values were measured without stirring, and considered stable following no change to the measurement after approximately 30 s (WTW auto-read function) (cf. Leito et al., 2002). The chemical changes were modelled using geochemical speciation software MIX4 (Plummer et al., 1975; Fairchild and Baker, 2012) and compared to changes in electroconductivity calculated using algorithms of Rossum et al. (1975) and Hughes et al. (1994). The change in $Ca^{2+}(aq)$ and $CO_3^{2-}(aq)$ composition in each growth chamber was calculated based on this established relationship between ionic strength with both pH and EC. Results showed some scatter around the calculated co-variation in these parameters (Fig. S2) and pH results were preferred because of the better analytical precision in relation to the magnitude of change. To compensate for these changes in solution composition and re-adjust the saturation state back to the original starting value, addition of 0.1 M NaOH was used to adjust the pH, and a mixed restoration solution of 0.1 M $CaCl_2$ and 0.2 M $NaHCO_3$ was used to replenish the Ca^{2+}, HCO_3^- and CO_3^{2-} ions in solution. Intervention with NaOH and restoration solution was undertaken on a daily or weekly timescale, dependent upon saturation state of the growth media and the rapidity of calcite precipitation. An example of an experiment with a weekly intervention is illustrated in Fig. 3: pH is repeatedly restored to the original value, but EC gradually rises because of accumulation of excess NaCl in solution. The change in pH prior to restoration was usually <0.1, but infrequently up to a maximum of 0.3, and the calcite saturation index (Ω = log ionic activity product over solubility product) was, correspondingly, lowered by 0.1–0.3.

Growth chambers were maintained until sufficient calcium carbonate had precipitated from solution for analysis. The precipitates were recovered from growth chambers by filtration. Crystals were imaged by Scanning Electron Microscopy (SEM), and rates of growth calculated by conversion of $CaCO_3$ precipitated (mg) during each experiment, to rates of linear extension in mm yr^{-1}. Crystal growth rates were similar to a sub-set of those of Mucci and Morse (1983) where calcite was grown under similar saturation states and Mg/Ca ratios (Fig. S3). Each of the recovered aliquots of calcite crystals were digested in 8 ml of 2% v/v HNO_3 (Aristar grade) and sulphur concentrations were determined by high-resolution inductively coupled plasma mass spectrometric analysis (HR-ICPMS) at Kingston University, UK, using methods described in Frisia et al. (2005). Calibration solutions at 1, 5, 10, 20, 50 and 100 ppb were diluted from a stock reference material of 1000 ppm sodium sulphate solution. Repeat analysis of the 10 ppb reference standard, tested as an unknown solution gave a sample precision to within <5% of the known concentration. Drift was monitored throughout the analytical sequence. Allowing for the mass of sulphate-free seed, the corrected sulphate concentration was determined and D_{SO_4} calculated from this value and the solution composition.

2.2. Cave site and speleothem sample descriptions

One speleothem was studied from each of two Alpine locations. Obir cave (SE Austria) lies within the Triassic limestone of the Obir Massif (46°30′36″N, 14°32′24″E, ~1100 m a.s.l.). The vegetation above the cave system is characterised by mixed deciduous/coniferous forest and well-developed brown earth soil extends to a depth of approximately 30 cm above the cave. Cave internal temperatures are +5.7 ± 0.1 °C and strong cave ventilation reflects the dominant seasonality of cave external temperatures (Spötl et al., 2005). Speleothem Obi84 was collected during 2002 and speleothem Obi12 was collected in 1998. Both samples have subsequently become noted for their seasonality of texture and geochemistry (Smith et al., 2009; Fairchild et al., 2010). Sulphur variations in speleothem Obi84 are apparent on both centennial and sub-annual scales (Wynn et al., 2010, 2014). The Ernesto cave system lies 220 km to the WSW (45°58′37″N, 11°39′28″E, 1167 m a.s.l) within the partially dolomitised Jurassic limestones of NE Italy. A similar vegetation composition of mixed deciduous/coniferous forest supports a clay-rich calcareous brown soil 0.5–1.5 m thick above the cave. The internal cave temperature is +6.7 ± 0.1 °C (Miorandi et al., 2010), and a strong seasonality in external temperature drives a cave ventilation pattern which holds a dominant influence over the cave carbon budget and speleothem growth patterns (Frisia et al., 2011). Speleothem ER78 was collected in 2000 and has been studied extensively for its sulphur content (Frisia et al., 2005; Wynn et al., 2010) and associated biogeochemical cycling of sulphur through the cave and overlying ecosystem (Wynn et al., 2013; Borsato et al., 2015).

Due to the broad similarities in climate regime, vegetation composition and cave ventilation dynamics at each cave site, both speleothems display similar trends in sulphur dynamics over the past 100 years. Analysis of both speleothem samples for sulphur content was undertaken at the European Synchrotron Radiation Facility (ESRF) at beamline ID21 in 2011 (Obi84) and 2003 (ER78). Analytical details are reported in Wynn et al. (2014) and Frisia et al. (2005) respectively. A rise in sulphur concentration throughout the 20th century is commensurate with a shift in isotopic composition signifying enhanced fossil fuel emissions (Wynn et al., 2010). Maximum concentrations of sulphur within each speleothem lag peak atmospheric emissions from industrialisation by approximately 10–15 years, attributed to biogeochemical attenuation within the overlying vegetation (Frisia et al., 2005; Wynn et al., 2010, 2013). High-resolution variability in sulphur concentration in the form of annual cycles, is superimposed on the long-term centennial sulphur trend in each speleothem (Frisia et al., 2005; Wynn et al., 2014). Cycles in sulphur

Table 1
Results from growth chamber experiments detailing experimental conditions and calculated partition coefficients.

Experiment number	pH[a]	Ω[b]	CO$_3$ (aq) (µM)[c]	HCO$_3$ (µM)[d]	γCO$_3$[e]	γHCO$_3$[f]	SO$_4$ (aq) (µM)[g]	SO$_4$/CO$_3$ (aq) (M)	SO$_4$ (mM) calcite[h]	SO$_4$/CO$_3$ calcite × 10^4	D$_{SO_4}$ × 10^5	LOG D$_{SO_4}$ × 10^5	Growth rate (mm yr^{-1})	LOG Growth rate (mm yr^{-1})
High aqueous sulphate (20 mg/l)														
C0.5N0.5-9.0	8.92 (8.78–9.0)	0.97 (0.79–1.07)	85.7 (60.5–103)	1665 (1647–1674)	0.755	0.93	208.2 (206.5–209.9)	2.43 (2.04–3.41)	6.8 (6.1–7.5)	6.8 (6.1–7.5)	28.1 (18.0–36.9)	1.45 (1.26–1.57)	0.43	−0.37
C1N1-8.6	8.43 (8.14–8.6)	1.05 (0.76–1.24)	63.1 (29.7–91.9)	3410 (3329–3470)	0.685	0.91	208.2 (206.5–209.9)	3.30 (2.28–6.95)	11.7 (10.7–12.6)	11.7 (10.7–12.6)	35.4 (15.4–55.3)	1.55 (1.19–1.74)	0.93	−0.03
C0.5N0.5-8.6	8.42 (8.17–8.6)	0.57 (0.31–0.71)	29.4 (14.3–42.4)	1703 (1675–1727)	0.76	0.93	208.2 (206.5–209.9)	7.08 (4.95–14.44)	7.5 (6.9–8.2)	7.5 (6.9–8.2)	10.65 (4.78–16.5)	1.03 (0.68–1.21)	0.07	−1.16
C1N1-8.3	8.24 (8.15–8.3)	0.87 (0.79–0.95)	37.1 (28.1–46.1)	3450 (3431–3470)	0.685	0.91	208.2 (206.5–209.9)	5.61 (4.55–7.35)	7.8 (7.0–8.5)	7.8 (7.0–8.5)	13.83 (9.55–18.7)	1.14 (0.98–1.27)	0.26	−0.59
C0.5N0.5-8.3	8.24 (8.13–8.3)	0.34 (0.23–0.42)	18.8 (14.4–21.3)	1720 (1710–1730)	0.76	0.93	208.2 (206.5–209.9)	11.07 (9.85–14.34)	6.0 (5.5–6.5)	6.0 (5.5–6.5)	5.4 (3.82–6.60)	0.73 (0.58–0.82)	0.02	−1.76
C1N1-8.0	7.84 (7.64–8.0)	0.5 (0.28–0.66)	17.7 (9.05–22.9)	3376 (3254–3450)	0.685	0.91	208.2 (206.5–209.9)	11.8 (9.16–22.8)	11.2 (10.4–12.1)	11.2 (10.4–12.1)	9.53 (4.53–13.2)	0.98 (0.66–1.12)	0.12	−0.92
C1.5N1.5-8.0	7.93 (7.81–8.0)	0.89 (0.75–0.96)	31.6 (23.8–36.0)	5120 (5020–5170)	0.64	0.89	208.2 (206.5–209.9)	6.6 (5.8–8.7)	12.4 (11.4–13.4)	12.4 (11.4–13.4)	18.8 (13.14–23.0)	1.28 (1.12–1.36)	0.49	−0.31
C1.51.5-7.5	7.46 (7.42–7.5)	0.4 (0.32–0.45)	9.89 (8.89–10.9)	4890 (4830–4950)	0.64	0.89	208.2 (206.5–209.9)	21.1 (19.3–23.2)	13.6 (12.6–14.6)	13.6 (12.6–14.6)	6.46 (5.40–7.60)	0.81 (0.73–0.88)	0.08	−1.10
Low aqueous sulphate (2 mg/l)														
C0.5N0.5-9.0	8.92 (8.78–9.0)	0.97 (0.79–1.07)	85.7 (60.5–103)	1665 (1647–1674)	0.755	0.93	20.8 (20.4–21.2)	0.24 (0.21–0.34)	2.6 (2.4–2.9)	2.63 (2.38–2.88)	108 (70.7–140)	2.03 (1.85–2.14)	0.51	−0.30
C1N1-8.6	8.43 (8.14–8.6)	1.05 (0.76–1.24)	63.1 (29.7–91.9)	3410 (3329–3470)	0.685	0.91	20.8 (20.4–21.2)	0.33 (0.23–0.69)	3.4 (3.1–3.6)	3.35 (3.07–3.64)	102 (44.6–157)	2.01 (1.65–2.20)	0.98	−0.01
C0.5N0.5-8.6	8.42 (8.16–8.6)	0.57 (0.31–0.71)	29.4 (13.7–42.4)	1703 (1674–1727)	0.755	0.93	20.8 (20.4–21.2)	0.71 (0.50–1.49)	3.3 (3.0–3.6)	3.29 (3.01–3.58)	46.5 (20.2–71.4)	1.67 (1.31–1.85)	0.06	−1.24
C1N1-8.3	8.24 (8.18–8.3)	0.87 (0.79–0.95)	37.1 (32.6–46.1)	3450 (3442–3470)	0.685	0.91	20.8 (20.4–21.2)	0.56 (0.46–0.63)	3.0 (2.7–3.3)	2.99 (2.67–3.31)	53.2 (42.6–71.9)	1.73 (1.63–1.86)	0.24	−0.63
C0.5N0.5-8.3	8.22 (8.08–8.3)	0.34 (0.23–0.42)	18.8 (13.0–21.3)	1720 (1700–1730)	0.755	0.93	20.8 (20.4–21.2)	1.11 (1.00–1.57)	2.4 (2.2–2.6)	2.41 (2.21–2.62)	21.8 (14.1–26.2)	1.34 (1.15–1.42)	0.02	−1.63
C1N1-8.0	7.84 (7.61–8.0)	0.5 (0.28–0.66)	17.7 (7.86–22.9)	3376 (3236–3450)	0.685	0.91	20.8 (20.4–21.2)	1.18 (0.93–2.60)	2.7 (2.5–3.0)	2.74 (2.53–2.95)	23.3 (9.73–31.9)	1.37 (0.99–1.5)	0.12	−0.91
C1.5N1.5-8.0	7.93 (7.81–8.0)	0.89 (0.75–0.96)	31.6 (23.8–36.0)	5120 (5020–5170)	0.64	0.89	20.8 (20.4–21.2)	0.66 (0.59–0.86)	2.8 (2.6–3.1)	2.80 (2.55–3.05)	42.4 (29.7–51.7)	1.63 (1.47–1.71)	0.49	−0.31
C1.5N1.5-7.5	7.46 (7.38–7.5)	0.4 (0.32–0.45)	9.89 (7.91–10.9)	4890 (4770–4950)	0.64	0.89	20.8 (20.4–21.2)	2.11 (1.95–2.58)	3.2 (3.0–3.5)	3.23 (2.98–3.48)	15.3 (11.6–17.9)	1.19 (1.06–1.25)	0.09	−1.07

Tabulated data are mean values, with the range associated with each parameter presented in parentheses.

[a-d] Mean values are weighted according to the mass of calcium carbonate precipitated in each experiment. The range represents the spread of values in each measured data set.

[e-f] Activity coefficients for HCO$_3^-$ and CO$_3^{2-}$ in solution were determined by PHREEQE and used to calculate both carbonate and bicarbonate ion concentration from the second dissociation constant for carbonic acid.

[g] The range of aqueous sulphate concentrations reflects the maximum systematic error associated with pipetting.

[h] The range of values associated with the sulphate content of product calcite are calculated based on an instrumental precision of 7.5% RSD from replicate analyses. Ω = log ionic activity product over solubility product.
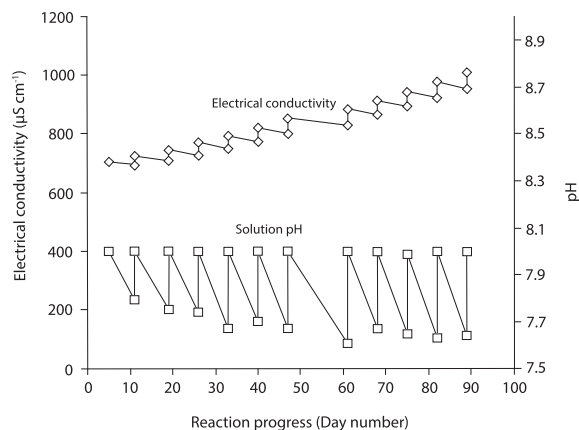
Fig. 3. Experimental progress of C1N1-8.0 depicting the drop in pH and EC between weekly interventions and solution restoration. The incremental rise in EC throughout the duration of the study reflects the use of a mixed restoration solution of 0.1 M $CaCl_2$ and 0.2 M $NaHCO_3$ to replenish the Ca^{2+}, HCO_3^- and CO_3^{2-} ions in solution, leading to accumulation of excess NaCl in solution.

concentration were confirmed as annual, based on the use of an age model for each speleothem developed using U-Th dating, visible lamina counting, and automated peak detection software developed by Smith et al. (2009). Annual pulses in Zn associated with colloidal movement during periods of April/September water excess for speleothem Obi84 (Fairchild et al., 2010; Hartland et al., 2011, 2012), and broadly synchronous changes in P (for speleothem ER78) (cf. Frisia et al., 2005; Borsato et al., 2007; Smith et al., 2009) were also used to further delimit the annual nature of sulphur cycles. Other cave sites where coeval speleothem extraction and drip water chemical monitoring allow the calculation of site-specific D_{SO_4} values include: Rukiesa cave, Ethiopia (Asrat et al., 2007, 2008; Baker et al., 2007); Crag Cave, Ireland (McDermott et al., 1999; Tooth and Fairchild, 2003; Baldini et al., 2006, 2008; Sherwin and Baldini, 2011); Uamh An Tartair, Scotland, UK (Proctor et al., 2000; Fuller et al., 2008, Baker et al., 2012); Browns Folly Mine, UK (Baker et al., 1998, 1999; Baldini et al., 2001, 2005; Fairchild et al., 2006); Shimizu-do cave, Japan; and Ryuo-do cave, Japan (Uchida et al., 2013). For each of these sites, drip water chemical monitoring is at a resolution lower than seasonal, and speleothem sulphur concentrations were determined only at low resolution incorporating several years of carbonate deposition from the most recent growth. Details of each of these sites is provided in the supplementary information.

3. RESULTS

Results from the growth chamber experiments are presented in Table 1, demonstrating the controls on sulphate incorporation into calcite. The pH control on absolute concentrations of sulphate incorporated during crystal growth is demonstrated in Fig. 4a. A negative relationship between sulphur concentration in calcite overgrowths and the pH of the growth media is apparent at high (20 ppm) concentrations of sulphate contained within the growth solution (p

= 0.044). This is consistent with the assumption that competition between sulphate and carbonate ions would force low levels of sulphate incorporation at high pH. The pH dependence of sulphate incorporation into calcite is limited in growth media of low sulphur concentration.

The substitution of carbonate by sulphate within the calcium carbonate lattice (Eq. (1)) suggests that elevated carbonate ion concentrations discourage sulphate incorporation. Therefore, sulphate incorporation rates should decrease by an order of magnitude relative to unit increases in pH (pH being an exponential scale, an increase in pH by one unit increases the CO_3/HCO_3 ratio by a factor of 10). However, sulphate incorporation only changes by a factor of 3 for every pH unit at 20 ppm aqueous sulphate and less than a factor of 2 for every pH unit at 2 ppm aqueous sulphate. This therefore results in a D_{SO_4} which increases with pH, suggesting a more efficient incorporation of sulphate into calcite at high pH and at low sulphur concentration
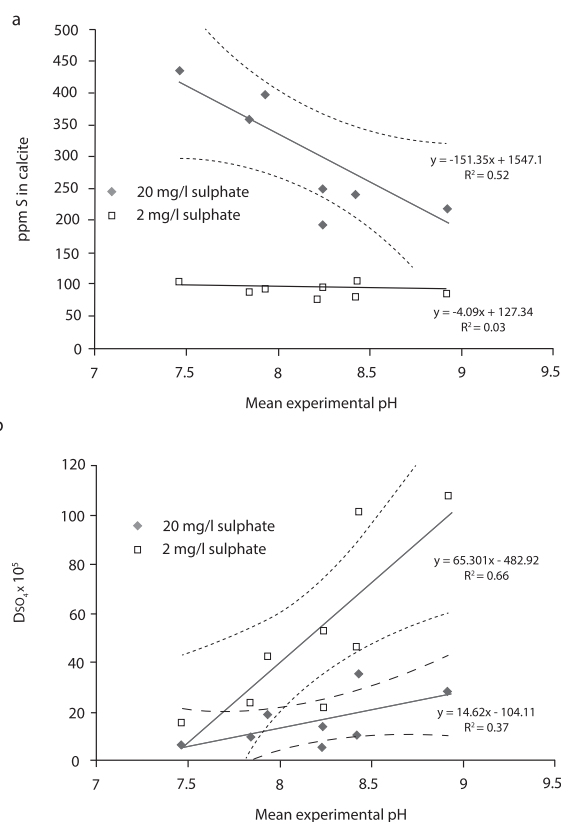

Fig. 4. The pH-dependence of sulphate incorporation into calcite. (a) Concentrations of sulphate incorporated into calcite demonstrate a negative relationship whereby the increasing abundance of carbonate ions at high pH limits the availability of sulphate in the calcite. The slope of the relationship is statistically significant for high (20 ppm) concentrations of sulphate in solution (ANOVA f-test, p = 0.044), but statistically indistinguishable for low (2 ppm) concentration experiments. (b) A positive relationship between D_{SO_4} and pH demonstrates a greater efficiency of incorporation under growth media conditions of high pH and low sulphur concentration, despite the lower abundance of sulphate ions in solution relative to carbonate (ANOVA f-test, p < 0.02 for high (20 ppm) and p < 0.05 for low (2 ppm) experimental series).

(Fig. 4b, p < 0.02 for high (20 ppm) and p < 0.05 for low (2 ppm) experimental series). A comparison of solutions with similar pH and differing saturation states reveals that the same positive relationship to D is expressed (Fig. 5, p < 0.05). Conditions of high pH, high supersaturation (driven independently of pH), and low sulphur concentration within experimental solutions thereby appear to promote a greater efficiency of sulphate incorporation into carbonate crystals.

Where records from cave drip water/pool water and speleothem sulphate analyses overlap, partition coefficients (expressed as values of D_{SO_4}) have been calculated. These are presented in Table 2 as average seasonal values for the Obir and Ernesto cave sites, and can be compared to the experimental data. Analysis of in-cave partition
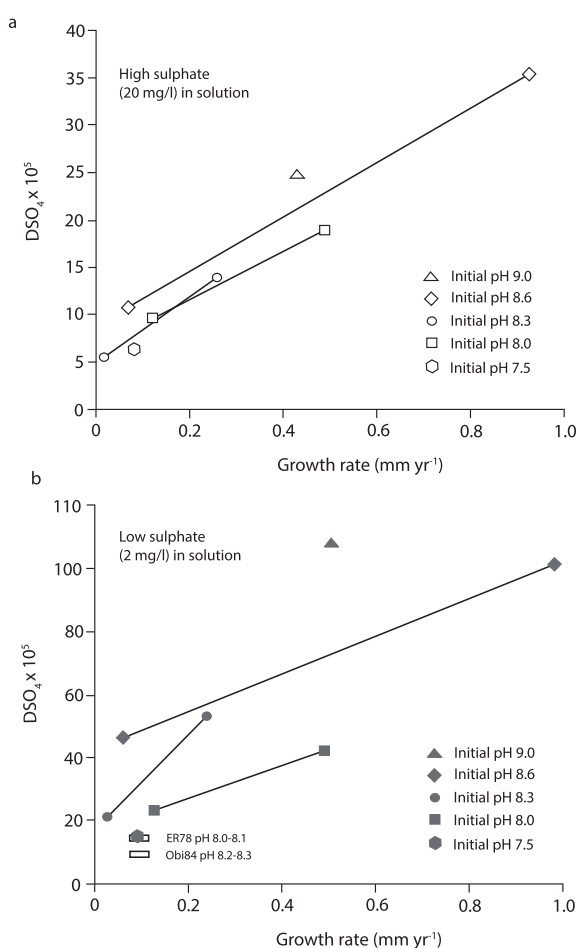

Fig. 5. The growth rate dependence of sulphate incorporation into calcite based on D_{SO_4}. At constant pH, a greater efficiency of sulphate incorporation is implied at faster rates of growth. Multiple linear regression demonstrates significance at the 0.05 level for both (a) high (20 ppm) sulphate experiments ($D_{SO_4} = -49.85 + 29.06$ growth rate + 6.90 pH; $r^2 = 0.95$), and (b) low (2 ppm) sulphate experiments ($D_{SO_4} = -336.17 + 61.11$ growth rate + 44.47 pH ($r^2 = 0.90$). Low sulphur experiments demonstrate greater efficiency of sulphate incorporation. Data points of constant pH are visually linked by solid black lines. Speleothems from Ernesto and Obir caves are plotted in Fig. 5b including dripwater pH values for comparison to experimental data.

coefficients is also extended to cave sites in other regions where coeval aqueous and speleothem carbonate sulphate analysis has been undertaken, albeit at a lower resolution of analysis (Tables 3 and 4).

4. DISCUSSION

4.1. Mechanisms of sulphate incorporation into experimental calcite

Sulphate incorporation into calcite has traditionally been determined to proceed by sulphate acting as a substituent for carbonate. Partition coefficients, expressed as D_{SO_4} (Eq. (1)) have thereby depicted the incorporation of sulphate to be driven at least in part by the aqueous SO_4/CO_3 ratio, controlled by pH and saturation state (Busenberg and Plummer, 1985). This relationship has been proved correct in a qualitative fashion (Fig. 4a), demonstrating the sulphate content of experimental calcite to decline with increasing pH when aqueous sulphate concentrations approximate 20 ppm. However, when aqueous sulphate concentrations approximate 2 ppm, the pH and saturation state control on sulphate incorporation into calcite is weak. This limited relationship reflects two confounding factors which expose the weakness of D_{SO_4} as a universal parameter, and reflect the deficiencies of the partition coefficient approach (Fairchild and Baker, 2012, ch. 8). These can be summarised as follows: 1. D_{SO_4} increases with pH (Fig. 4b), offsetting the expected decline in calcite sulphate content (Eq. (1)). 2. At constant pH, growth rate is driven by supersaturation and an associated increase in D_{SO_4} with growth rate is demonstrated (Fig. 5a, b). These deviations from the partition co-efficient approach suggest multiple controls to anion substitution into calcium carbonate (cf. Uchikawa et al., 2017) indicating a dual model to sulphate incorporation comprising A. Substitution of carbonate for sulphate following partition coefficient behaviour (cf. Busenberg and Plummer, 1985), albeit modified to account for the effects of bicarbonate competition on the calcite surface (Andersson et al., 2016); and B. Possible incorporation of sulphate into the solid-state lattice at defect sites (cf. Pingitore and Eastman, 1986; Staudt et al., 1994).

Bicarbonate competition on the calcite surface: Traditional models of partition co-efficient behaviour concerning carbonate ion abundance do not consider the effects of a bicarbonate competition for space within the calcite lattice. The partition co-efficent (D_{SO_4}), as defined through Eq. (1), assumes all carbonate which contributes to the growth of calcite crystals is deposited directly onto the growth surface as CO_3^{2-} ions (Eq. (1)). However, both HCO_3^- and CO_3^{2-} are capable of contributing to calcite growth, by diffusing towards and attaching to the growth surface of $CaCO_3$ crystals (eg. Przybylinski, 1987; Van der Weijden et al., 1997; van der Weijden and van der Weijden, 2014). The subsequent deprotonation of bicarbonate adsorbed to and/or incorporated within the calcite lattice to produce carbonate ions has a pK_a value which is less than free bicarbonate in solution (Andersson et al., 2016). This means the calcite surface preferentially stabilizes carbonate ions

Table 2
Seasonal partition coefficients between cave waters and speleothem calcite at the Obir and Ernesto cave systems.

Cave water sample	Dripwater pH[a]	Dripwater CO₃ (µM)[b]	Dripwater HCO₃ (mM)[c]	Dripwater SO₄ (µM)[d]	Dripwater SO₄/CO₃	SO₄ (mM) in coeval speleothem calcite[e]	SO₄/CO₃ Speleothem calcite × 10⁴	D_{SO_4} × 10⁵[f]	Speleothem growth rate (LOG mm/yr)	Expected D_{SO_4} × 10⁵[g]
Obir cave[*]										
Winter average	8.30 (8.17–8.42)	40.8 (30.9–53.3)	3.0 (2.8–3.2)	46.9 (46.9–46.9)	1.2 (0.9–1.5)	1.3 (1.2–1.4)	1.3 (1.2–1.4)	11.1 (7.8–15.6)	−0.89	11.7–36.6
Summer average	8.15 (8.07–8.23)	29.7 (24.9–33.4)	3.2 (3.0–3.2)	46.9 (46.9–46.9)	1.6 (1.4–1.9)	1.4 (1.3–1.5)	1.4 (1.3–1.5)	9.0 (6.9–10.8)	−1.15	8.7–28.3
Ernesto Cave[**]										
Winter average	8.14 (7.94–8.33)	25.3 (12.5–41.0)	2.5 (2.15–2.88)	69.1 (65.7–71.0)	2.7 (1.7–5.3)	4.2 (3.9–4.5)	4.2 (3.9–4.5)	15.4 (7.4–26.1)	−0.89	11.7–36.6
Summer average	8.02 (7.84–8.14)	18.8 (12.7–27.4)	2.7 (2.14–3.03)	70.5 (65.3–72.6)	3.8 (2.7–5.1)	5.6 (5.2–6.0)	5.6 (5.2–6.0)	14.9 (10.0–22.6)	−1.15	8.7–28.3

Tabulated data are mean values, with the range associated with each parameter presented in parentheses.

[a-d] Range represents the spread of values in each measured data set.

[e] The range of values associated with the sulphate content of speleothem calcite are calculated based on an instrumental precision of 7.5% RSD from replicate analyses.

[f] The range in D_{SO_4} × 10⁵ is calculated based on measured environmental parameters, including 7.5% RSD from [e] instrumental precision.

[g] The range in expected D_{SO_4} is calculated from the experimental data on sulphate partitioning extrapolated to appropriate growth rates (Fig. 8) at low (2 ppm) and high (20 ppm) aqueous sulphate concentrations. Seasonal differences in D_{SO_4} × 10⁵ are statistically significant (p = 0.045, Mann Whitney U-test) at Obir cave, although at Ernesto cave D_{SO_4} values are statistically indistinguishable between summer and winter seasons.

[*] Obir cave waters represent average values for both summer and winter seasons throughout 2002–2004. Coeval speleothem calcite for this site represents the year 2000.

[**] Ernesto cave waters represent average values for both summer and winter seasons throughout 1996–1997. Coeval speleothem calcite for this site represents the year 1996.

Table 3
Calculated partition coefficients between cave waters and speleothem calcite at a range of cave systems, demonstrating the universal applicability of experimentally determined partition coefficient D_{SO_4}. All data prefixed a-g are referenced through Table 4.

Speleothem sample	Drip water pH[a]	Drip water CO₃ (µM)[b]	Dripwater HCO₃ (mM)[c]	Drip water SO₄ (µM)[d]	Drip water SO₄/CO₃	SO₄ (mM) in speleothem calcite[e]	SO₄/CO₃ speleothem calcite × 10⁴	D_{SO_4} × 10⁵[f]	Speleothem growth rate (LOG mm/yr)[g]	Expected D_{SO_4} × 10⁵[h]
ASFA 3	7.81 (7.47–8.15)	30.3 (5.9–100.9)	7.0 (3.2–10.7)	115.6 (112.1–125.1)	3.8 (19.1–1.2)	5.0 (4.6–5.3)	5.0 (4.6–5.3)	13.0 (2.4–43.1)	-0.52	14.4–44.2
MERC-1	7.81 (7.47–8.15)	24.7 (2.7–100.2)	6.2 (1.5–10.7)	37.2 (27.8–50.9)	1.51 (10.2–0.5)	2.5 (2.3–2.7)	2.5 (2.3–2.7)	16.3 (2.2–52.2)	-0.52	14.4–44.2
CC-BIL	7.50 (7.30–7.70)	10.6 (4.8–20.9)	5.0 (3.6–6.3)	21.56 (21.7–21.7)	2.03 (4.6–1.0)	6.0 (5.5–6.4)	6.0 (5.5–6.4)	29.3 (12.1–62.1)	-0.37	20.8–61.0
SU96-7	8.26 (7.70–8.93)	56.1 (14.9–252.6)	5.0 (5.0–5.0)	54.8 (46.9–66.5)	1.0 (3.1–0.3)	1.0 (0.9–1.1)	1.0 (0.9–0.1)	10.1 (2.9–40.2)	-1	8.1–26.4
BFM-Boss	7.94 (7.31–8.40)	30.6 (4.8–121.1)	4.7 (3.5–7.3)	114.3 (64.7–200.1)	3.7 (13.4–1.7)	7.0 (6.5–7.5)	7.0 (6.5–7.5)	18.7 (4.8–45.5)	-0.55	17.0–51.0
Obi12	8.19 (8.04–8.34)	30.0 (19.9–45.1)	3.2 (3.0–3.3)	55.1 (50.5–59.7)	1.8 (2.5–1.3)	1.9 (1.7–2.0)	1.9 (1.73–2.01)	10.2 (6.8–15.2)	-1	10.3–32.9
Shimizu-do B1	7.76 (7.57–8.18)	14.5 (6.6–49.7)	3.8 (2.9–5.0)	97.9 (93.7–104.2)	6.7 (14.1–2.1)	5.7 (5.4–6.0)	5.7 (5.4–6.0)	8.5 (3.9–28.7)	-1.46	6.2–21.0
Ryuo-do-R1	8.08 (7.82–8.29)	18.0 (9.3–36.6)	2.4 (2.2–3.0)	154.1 (145–168)	8.6 (15.6–4.6)	5.5 (5.2–5.7)	5.5 (5.2–5.7)	6.4 (3.3–12.5)	-1.14	9.2–29.5

Tabulated data are mean values, with the range associated with each parameter presented in parentheses.

[a-d] Range represents the spread of values in each measured data set.

[e] The range of values associated with the sulphate content of speleothem calcite are calculated based on an instrumental precision of 7.5% RSD from replicate analyses.

[f] The range in D_{SO_4} × 10⁵ is calculated based on pairing min and max values of SO₄ and CO₃ in each of the measured data sets.

[g] Growth rates are obtained from sources listed in Table 4.

[h] The range in expected D_{SO_4} is calculated from the experimental data on sulphate partitioning extrapolated to appropriate growth rates (Fig. 8) at low (2 ppm) and high (20 ppm) aqueous sulphate concentrations.

Table 4
Speleothem sample details and data sources associated with cave sites presented in Table 3.

Speleothem code	Cave details	Data source
ASFA 3	Rukiesa cave, Ethiopia. Asfa chamber	a Asrat et al., 2008; b-c Baker et al., 2007; d-e Data source this publication; f Asrat et al., 2008; g calculated from LOG growth rate based on Fig. 8
MERC-1	Rukiesa cave, Ethiopia. Merc chamber	a-c Asrat et al., 2008; d-e Data source this publication; f Asrat et al., 2008; g calculated from LOG growth rate based on Fig. 8
CC-BIL	Crag cave, Ireland	a-c Baldini et al., 2006; d Data source this publication; e Wynn et al., 2008; f Baldini et al., 2008; g calculated from LOG growth rate based on Fig. 8
Assynt	Uamh Am Tartair, Assynt, UK	a-d Fuller et al., 2006; e Data source this publication; f Proctor et al., 2000; g calculated from LOG growth rate based on Fig. 8
BFM-Boss	Browns Folly Mine, UK	a-d Data source this publication; e Wynn et al., 2008; f Data source this publication g calculated from LOG growth rate based on Fig. 8
Obi 12	Obir cave, Austria. Saulenhalle chamber	a-d Fairchild et al., 2010; e Data source this publication; f Fairchild et al., 2010; g calculated from LOG growth rate based on Fig. 8
Shimizu-do B	Shimizu-do cave, Japan. Stalagmite B	a-f Uchida et al., 2013; g calculated from LOG growth rate based on Fig. 8
Ryuo-do-R1	Ryuo-do cave, Japan	a-f Uchida et al., 2013; g calculated from LOG growth rate based on Fig. 8

a = drip water pH, b = drip water carbonate, c = drip water bicarbonate, d = drip water sulphate concentration, e = sulphate concentration in speleothem calcite from the most recent growth, f = speleothem growth rate, g = expected range in D_{SO_4} calculated from experimental data on sulphate partitioning extrapolated to appropriate growth rates at low (2 ppm) and high (20 ppm) aqueous sulphate concentrations.

relative to bicarbonate, leaving only low concentrations of bicarbonate ions present within the lattice (Feng et al., 2006) despite much higher concentrations within the aqueous phase. The values of pK_a for deprotonation of HCO_3 to CO_3 on the surface of calcite vary by six orders of magnitude depending on pH and calcite surface geometry. However, at the pH values present within natural cave environments (encompassing those used within the present study), values of pK_a suggest virtually complete deprotonation regardless of calcite surface conditions (Andersson et al., 2016). This leads to competition between bicarbonate and sulphate for space within the calcite lattice, which is determined by solution pH and relative bicarbonate ion abundance. At high pH (higher than 10.3), where carbonate ions in solution are more abundant, the effects of bicarbonate competition are limited and D_{SO_4} should be close to the true value as calculated through Eq. (1). At the range of pH conditions conducive to a greater dominance of bicarbonate ions in solution (between pH 6.4 and 10.3), 'bicarbonate competition' with sulphate for spaces within the calcite lattice serves to dilute the incorporation of the sulphate molecule, thereby introducing uncertainty into the partition coefficient calculation of Eq. (1). This results in a lower D_{SO_4} than expected from Eq. (1) and reflects the relationship to pH depicted through Fig. 4b.

Defect site abundance: The abundance of defect sites in calcium carbonate crystals is directly related to supersaturation state and therefore crystal nucleation and growth (McDermott et al., 1999; Frisia et al., 2000). An enhanced presence of defect sites (visible as stepped crystal faces) is known to encourage exchange of ions between aqueous and solid phases (Pingitore and Eastman, 1986; Staudt et al., 1994; Borsato et al., 2016; Uchikawa et al., 2017). Therefore, increased defect site density at higher supersaturation states promotes sulphate incorporation (increasing D_{SO_4}) (Fig. 6), and is manifested through increasing D_{SO_4} with both pH (Fig. 4b) and higher growth rates when pH remains constant (Fig. 5a-b).

The net effects of all these processes (partitioning according to carbonate ion abundance; competition with

bicarbonate; the presence of defect sites; and the absolute concentrations of sulphate in solution) are depicted through Fig. 7. The apparent increase in calcite sulphur content with growth rate (Fig. 7) is counter-intuitive based on a model of sulphate incorporation controlled solely by carbonate ion abundance in solution (Eq. (1)). Instead, sulphate incorporation at defect sites must increase D_{SO_4} and offset the effects of carbonate ion abundance. The strength of this overall growth rate effect is modest, exhibiting a ~20% increase in sulphur concentration in calcite over an order of magnitude growth rate increase along a line of constant pH (at 20 ppm sulphate solution, significant at the p = 0.05 level). At lower sulphate concentrations in solution (2 ppm), the same effect of enhanced sulphur incorporation into calcite with growth rate offsets the expected dilution by carbonate ion abundance but does not display a positive trend. At similar rates of growth, the effect of pH upon sulphur incorporation into calcite follows the relationship depicted through Fig. 4a, whereby pH control of aqueous SO_4/CO_3 ratio determines the abundance of sulphate incorporated into calcite despite any effects of variable D_{SO_4}.

4.2. Comparison to published experimental data

The only other study to date investigating partitioning of sulphate into calcite (Busenberg and Plummer, 1985) addressed crystal growth rates predominantly faster than those encountered during speleothem deposition (linear extension rates equivalent to 0.3–40 mm/year). Additionally, experimental solutions used concentrations of sulphate and sodium one to two orders of magnitude greater than those typical of karst environments. The relationship between crystal growth rate and partition coefficient is depicted through Fig. 8 as a linear expression relating LOG(D) to LOG(R) (p = 9.0×10^{-13}, where LOG(R) is LOG growth rate in mm extension per year).

$$LOG(D) = 0.8098 * LOG(R) - 0.1446 \qquad (2)$$

Extrapolating the linear relationship in Eq. (2) to a growth rate of 100 µm yr^{-1}, should yield a D_{SO_4} value
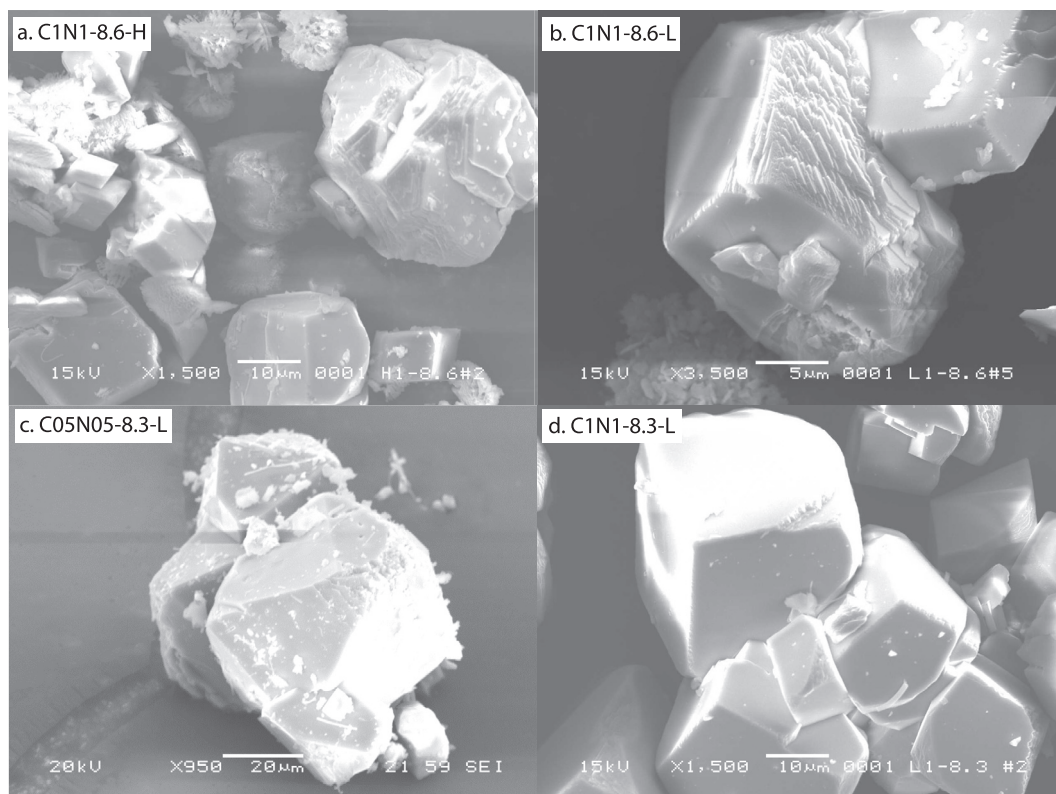
Fig. 6. SEM images of product calcite crystals showing the presence of defect sites (visible as stepped crystal faces) grown across a range of saturation indices and pH values. Images shown relate to experimental products from (a) incubation C1N1 at pH 8.6 for 20 ppm aqueous sulphate concentration, (b) incubation C1N1 at pH 8.6 for 2 ppm aqueous sulphate concentration, (c) incubation C1N1 at pH 8.3 for 2 ppm aqueous sulphate, and (d) incubation C05N05 at pH 8.3 for 2 ppm aqueous sulphate concentration. Further information on experimental conditions associated with each incubation are available through Table 1.

$(\times 10^5)$ of 0.1. This is much lower than the values of D_{SO_4} obtained as a part of this study for similar rates of growth. At low (2 ppm) sulphur concentrations, $D_{SO_4} \times 10^5 = 32.9$, whereas at higher concentrations of sulphate (20 ppm), $D_{SO_4} \times 10^5 = 10.3$. The greater efficiency of trace element incorporation in this study and at lower concentrations of sulphate may reflect the lower ionic strength of the growth media. Difficulties in extrapolating partition coefficients beyond the studied range of solution composition has also been demonstrated for other trace elements such as Sr, Cd, Mn and Co during incorporation into calcite (e.g. Lorens, 1981).

4.3. Mechanisms of sulphate incorporation into speleothem calcite

The proposed model of pH and defect control on sulphate incorporation into experimental calcite is consistent with observations of sulphate variability contained within speleothem carbonate. Where cave ventilation serves as the main driver of drip water pH, the incorporation of sulphate into the speleothem is modulated according to levels of CO_2 in the cave atmosphere (Frisia et al., 2005). Where ventilation occurs on a seasonal basis, this process gives rise to annual cycles of speleothem sulphate content despite relatively constant sulphate concentrations within cave drip waters across an annual cycle (Borsato et al., 2015). Minimal amounts of sulphate incorporation into speleothem carbonate always occur during ingress of external air with low PCO_2 into the cave chamber (therefore drip waters de-gas to attain a relatively high pH), and maximum levels of sulphate are incorporated in speleothem carbonate during egress of cave air when high ambient levels of cave air CO_2 reduce drip water degassing and thus limit the pH attained to lower values. At the Obir and Ernesto cave systems, this gives rise to a winter low and a summer high in speleothem sulphate concentration. However, if pH-determined sulphate substitution for carbonate were the sole controlling variable on sulphate incorporation into calcite, the seasonal cycle of speleothem sulphate would be expected to demonstrate a rapid switch between max and min concentrations in accordance with the rapidity of changes in cave ventilation regime. In reality, when analysed at high resolution (1 μm spatial resolution), the annual sulphate cycle appears blurred between max and min concentrations, contrasting with very sharp colloidal element bands (Fig. 1). This is likely due to gradual changes in the crystal growth surface and defect site availability, transitioning from high abundance of defects during the winter season to fewer defects during the summer over a time period which is slower than the switch in cave air CO_2 concentration (sensu Pingitore and Eastman, 1986; Borsato et al.,
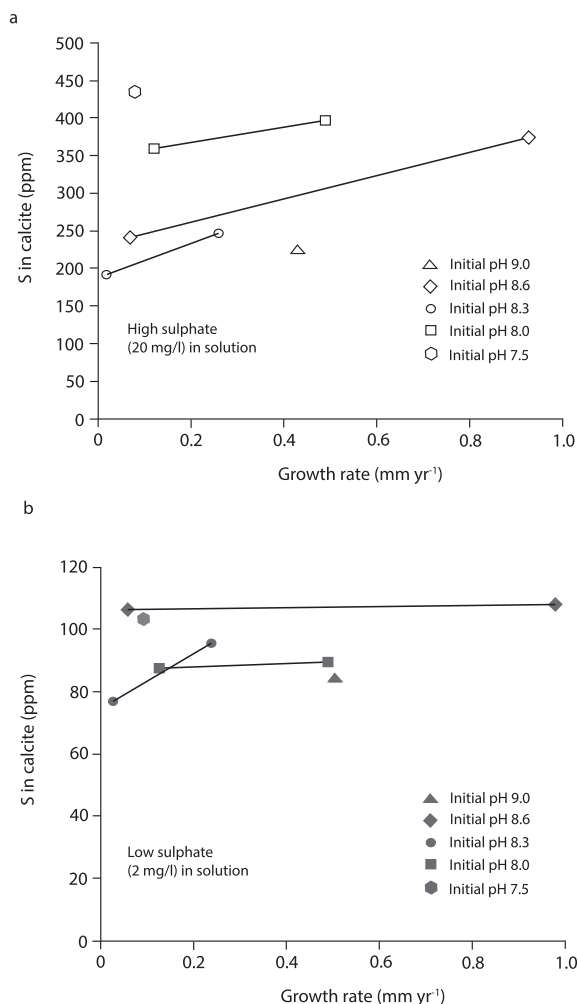
Fig. 7. The growth rate dependence of sulphate incorporation into calcite. At constant pH, a greater quantity of sulphate is incorporated at faster rates of growth. Multiple linear regression demonstrates significance at the 0.05 level for (a) high (20 ppm) sulphate experiments (S in calcite = 1828.89 + 201.45 growth rate − 190.75 pH; r^2 = 0.790), and no statistical significance at (b) low (2 ppm) sulphate experiments.

Fig. 8. The relationship between growth rate and partition coefficient depicted as a linear expression relating LOG(D) to LOG(R). Data obtained from Busenberg and Plummer (1985) where sulphate concentrations range between 100 and 10,000 ppm in solution (ANOVA f-test, p = 9.0×10^{-13}), and this study for high (20 ppm, ANOVA f-test p = 0.00071) and low (2 ppm, ANOVA f-test p = 0.03) sulphate experiments.

2016). This is associated with classic seasonal changes in the morphology of crystals growing on glass plates beneath drips in Ernesto cave (Frisia et al., 2000). Seasonally modulated supersaturation control on defect site availability and therefore D_{SO_4}, thereby serves to modify the dominant pH control on sulphate substitution for carbonate.

4.4. In-cave partitioning of sulphate between cave water and speleothem calcite

Where time series of cave pool water/drip water chemical analyses are temporally closely matched to speleothem records of sulphur concentration, the calculated partition coefficients between cave waters and speleothem calcite are directly comparable with those calculated through growth chamber experiments. This is undertaken at the Obir and Ernesto caves, where the frequency of drip water
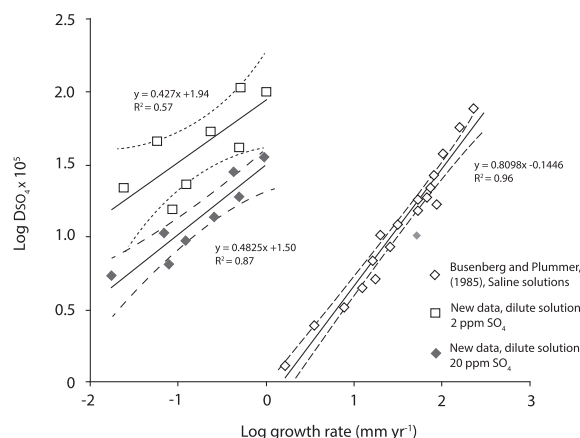
collection and the high resolution of speleothem sulphur analysis allow determination of D_{SO_4} on a seasonal basis.

The seasonality of dripwater SO_4/CO_3 characteristics reflect the cave ventilation dynamics (and thereby dripwater pH) at each site. At Obir cave, drip waters feeding speleothem Obi84 demonstrate a strong seasonality in drip water pH and SO_4/CO_3 ratios. During the winter season (defined as October–March), higher pH and consequently lower SO_4/CO_3 (mean pH = 8.3, mean SO_4/CO_3 = 1.2) contrasts with those values from the summer season (mean pH = 8.15, mean SO_4/CO_3 = 1.6) (Table 2). In Ernesto cave, calculations were performed on waters collected from Pool S1, the closest sampling site in the cave to the drip which fed stalagmite ER78. Seasonality in pH and SO_4/CO_3 ratios reflect a similar pattern of cave ventilation-modulated carbonate precipitation as that found in Obir cave. During the winter season, pool water chemistry dictates a lower SO_4/CO_3 ratio as a result of elevated pH and Ω (mean pH = 8.14, mean SO_4/CO_3 = 2.7). During the summer, lower drip water pH and Ω result in a higher SO_4/CO_3 ratio (mean pH = 8.0, mean SO_4/CO_3 = 3.8) (Table 2). This variability in pH and SO_4/CO_3 ratio drives the seasonally modulated cycles of speleothem sulphate as discussed above.

To enable sulphate partition co-efficients to be calculated between dripwaters and speleothem calcite, values of sulphate concentration in speleothem calcite were obtained at high resolution using raw counts generated by synchrotron XRF calibrated to analyses undertaken by secondary ionisation mass spectrometry (for speleothem Obi84) (Wynn et al., 2010) and high resolution ICPMS (for speleothem ER78) (Frisia et al., 2005). Concentrations of sulphate incorporated into speleothem calcite during the summer and winter seasons of each respective year were calculated as mean values based on the understanding that drip water Ca concentration indicates a 1.8x slower speleothem growth rate during the summer season. For

Obi84, drip water chemistry from 2002 to 2004 is compared to speleothem sulphate concentrations from the nearest full annual cycle in the synchrotron sulphur profile (year 2000). For ER78, drip water chemistry monitored between 1996 and 1997 is compared only to the year 1996 due to a poor cyclical structure in the synchrotron sulphur profile from 1997. Based on the growth chamber experiments reported above, partitioning of sulphate between cave waters and speleothem calcite should follow a relationship such that values of D_{SO_4} are enhanced at higher pH. At Obir cave, values of D_{SO_4} ($\times 10^5$) range between a winter mean of 11.1 to summer mean of 9.0 (Table 2, p = 0.045). At Ernesto cave, seasonal mean values of D_{SO_4} ($x10^5$) are calculated as 15.4 (winter) and 14.9 (summer), albeit statistically indistinguishable between summer and winter seasons. These values are close to the predicted values of D_{SO_4} based on chamber experiments containing both low (2 ppm) and high (20 ppm) sulphate concentrations and with crystal growth rates extrapolated to equivalent rates of linear extension (Table 2).

The partition co-efficients calculated between drip water and speleothem calcite can be interpreted based on experimental observations. Despite the lower concentrations of sulphate incorporated into speleothem calcite at higher pH values during the winter season (hence the origin of the annual speleothem sulphur cycles), values of D_{SO_4} reflect a greater efficiency of sulphate incorporation. This is hypothesized above to be due to an enhanced proportion of defects and kink sites at high levels of supersaturation that accommodate the sulphate ion (cf. Staudt et al., 1994). The increasingly defect-rich nature of crystal faces with increasing supersaturation state closely resembles processes of in-cave crystal formation, whereby winter growth at higher supersaturation promotes the formation of crystals with macro-kinks and steps (Frisia et al., 2000). However, given the modest increase in the sulphate content of experimental calcites over an order of magnitude increase in growth rate at constant pH (Fig. 7), the enhanced incorporation of sulphate at defect sites will not significantly diminish the over-riding pH control on SO_4/CO_3^- in product calcite. The growth chamber experiments of this study and Busenberg and Plummer (1985), thereby support a seasonality to sulphate incorporation in the speleothem record by identifying drip water pH (and by implication a pH-driven speleothem growth rate) as the key variable in determining the seasonality to sulphate incorporation and the magnitude of the partition coefficient (D_{SO_4}).

4.5. Universal applicability of speleothem D_{SO_4}

The universal applicability of D_{SO_4} to speleothems growing within the experimental range of crystal growth rates and aqueous sulphate concentrations is demonstrated in Table 3. For each speleothem, D_{SO_4} is derived from field data collected at low temporal sampling resolution. Drip water chemical composition (pH, carbonate and sulphate content) is reported as annual mean values broadly contemporaneous with the date of speleothem collection. Speleothem growth rate is reported as an annual average value over the past 100 years, and sulphate content is

reported from the most recent speleothem growth. Each calculated value of mean speleothem D_{SO_4} is seen to lie close to the range of experimentally determined partition coefficients when extrapolated to equivalent growth rates (Fig. 8) at low (2 ppm) and high (20 ppm) aqueous sulphate concentrations. The partitioning of sulphate between cave waters and speleothem calcite thereby appears to conform to experimentally determined controls across a range of environmental settings and temporal scales.

4.6. Speleothem sulphate concentrations as indicators of past climatic variability

The pH-dependence of sulphate incorporation into calcite and the universal relationship between growth rate (expressed as mm yr^{-1} linear extension) and D_{SO_4}, are two important findings which should permit the application of speleothem sulphate concentrations as climate proxies. These findings can be detailed as: 1. In a cave setting, the pH to which drip waters degas is controlled by the PCO_2 of the cave air and therefore ventilation regime. The shape of each seasonal sulphate cycle (specifically cycle length) observed in speleothem calcite should therefore reflect the nature and timing of ventilation at each site. At sites where temperature-driven density differences control cave air PCO_2, a temperature decline occurring unusually early in the autumn or a temperature rise unusually late in the spring would produce an extended winter circulation pattern associated with low sulphate levels and an associated change in the morphology of the sulphur peak-trough trace. 2. Based on the relationship between D_{SO_4} and growth rate (expressed as mm yr^{-1} linear extension) the partition coefficient between drip water and speleothem calcite can be predicted for different speleothems beyond the period of contemporary cave monitoring. Assuming an essentially constant pre-industrial sulphate flux to the stalagmite, D_{SO_4} variability should therefore reveal changes in drip water pH and by implication the relative strength of cave ventilation and external temperature dynamics over a range of timescales. However, both of these linkages to climate rely on minimal upstream changes in drip water sulphate and carbonate concentration induced by prior calcite precipitation (PCP), (cf. Borsato et al., 2016). Where PCP is apparent, the associated removal of carbonate from the drip water will tend to cause the aqueous sulphate/carbonate to rise. If the calcium carbonate precipitation was stimulated by a winter fall in CO_2 (rise in pH), the PCP effect will oppose the fall in speleothem sulphate that would otherwise be the hallmark of the seasonal change. PCP would therefore diminish the magnitude and duration of seasonal cycles in speleothem sulphate content. When the relationship between D_{SO_4} and speleothem growth rate is used to infer past changes in drip water pH, PCP would serve to disrupt this relationship. For the Ernesto cave system where PCP is of minimal significance, seasonal cycles in sulphate concentration and reconstructed values of D_{SO_4} can be used to infer changing environmental conditions as detailed above. However, when PCP plays a significant role in modifying drip water SO_4/CO_3 content, other proxies of PCP (Mg/Ca and Sr/Ca in speleothem carbonate, Fairchild

et al., 2000) need to be used to identify the extent of the process and the suitability of the sulphate record for environmental reconstruction. Consequently, when PCP can be deemed negligible or accounted for, both the pH driver of sulphate incorporation and the universal relationship between D_{SO_4} and growth rate therefore raise the possibility of using speleothem sulphate content as a proxy for changing seasonality in different environmental settings. When used as part of a multi-proxy approach, sulphate thereby promises to enhance the resolving power of speleothem archives of environmental change.

5. CONCLUSIONS

Calcite grown under controlled laboratory conditions provides the first quantitative description of the controls on annual cycles in speleothem sulphate. pH is confirmed as the dominant variable controlling the overall abundance of sulphate incorporated into calcite. The efficiency of sulphate incorporation into calcite (D_{SO_4}) is enhanced at high pH, high crystal growth rate and low sulphate concentrations in aqueous media. Increased D_{SO_4}, despite the lower sulphate ion abundance, probably reflects an increase in defect sites at calcite crystal surfaces associated with high levels of supersaturation, as well as bicarbonate competition at the calcite surface. In most cave environments, drip water pH is controlled by ventilation dynamics. Where cave ventilation is seasonal, the associated speleothem calcite will demonstrate a seasonality to sulphate incorporation. At the Obir and Ernesto caves, cave ventilation control of pH leads to characteristic summer peaks and winter lows in speleothem sulphate content. Increased crystal defects and limited bicarbonate competition associated with high levels of supersaturation during the winter season (low cave air PCO_2), likely explain the greater efficiency of sulphate incorporation at this time of year despite a lower SO_4/CO_3 ion abundance in drip waters. These same defect-rich crystallites are also responsible for the blurred transition in sulphur concentration between summer and winter seasons in the speleothem record. The experimental values of D_{SO_4} generated as a part of this study quantitatively reflect the incorporation of sulphate into contemporary speleothem calcite for stalagmites which have grown in a range of cave settings. Due to the universal applicability of the relationship between speleothem growth rate and D_{SO_4}, this opens the possibility of using speleothem records to reconstruct environmental drivers of sulphate partitioning, namely cave ventilation and external temperature dynamics across well-defined climatic changes where the effects of PCP are absent or can be accounted for.

ACKNOWLEDGEMENTS

APPENDIX A. SUPPLEMENTARY MATERIAL

Supplementary data associated with this article can be found, in the online version, at https://doi.org/10.1016/j.gca.2018.01.020.

REFERENCES

Andersson M. P., Rodriguez-Blanco J. D. and Stipp S. L. S. (2016) Is bicarbonate stable in and on the calcite surface? *Geochim. Cosmochim. Acta* **176**, 198–205.

Asrat A., Baker A., Umer M. M., Leng M. J., Van Calsteren P. and Smith C. (2007) A high-resolution multi-proxy stalagmite record from Mechara, Southeastern Ethiopia: palaeohydrological implications for speleothem paleoclimate reconstruction. *J. Quat. Sci.* **22**, 53–63.

Asrat A., Baker A., Leng M. J., Gunn J. and Umer M. (2008) Environmental monitoring in the Mechara caves, Southeastern Ethiopia: implications for speleothem paleoclimate studies. *Int. J. Speleol.* **37**(3), 207–220.

Badertscher S., Borsato A., Frisia S., Cheng H., Edwards R. L., Tüysüz O. and Fleitmann D. (2014) Speleothems as sensitive recorders of volcanic eruptions – the Bronze Age Minoan eruption recorded in a stalagmite from Turkey. *Earth Planet. Sci. Lett.* **392**, 58–66.

Baker A., Genty D., Dreybodt W., Barnes W., Mockler N. and Grapes J. (1998) Testing theoretically predicted stalagmite growth rate with recently annually laminated samples: implications for past stalagmite deposition. *Geochim. Cosmochim. Acta* **62**, 393–404.

Baker A., Mockler N. and Barnes W. (1999) Fluorescence intensity variations of speleothem forming groundwaters: implications for paleoclimate reconstruction. *Water Resour. Res.* **35**, 407–413.

Baker A., Asrat A., Fairchild I. J., Leng M. J., Wynn P. M., Bryant C., Genty D. and Umer M. (2007) Analysis of the climate signal contained within $\delta^{18}O$ and growth rate parameters in two Ethiopian stalagmites. *Geochim. Cosmochim. Acta* **71**, 2975–2988.

Baker A., Smith C. L., Jex C., Fairchild I. J., Genty D. and Fuller L. (2008) Annually laminated speleothems: a review. *Int. J. Spel.* **37**, 193–206.

Baker A., Bradely C., Phipps S. J., Fischer M., Fairchild I. J., Fuller L., Spötl C. and Azcurra C. (2012) Millennial-length forward models and pseudoproxies of stalagmite $\delta^{18}O$: an example from NW Scotland. *Clim. Past* **8**, 1153–1167.

Baldini J. et al. (2001) Morphological and dimensional linkage between recently deposited speleothems and drip water from Browns Folly Mine, Wiltshire, England. *J. Cave Karst Stud.* **63**, 83–90.

Baldini J. U. L., McDermott F., Baker A., Baldini L. M., Mattey D. P. and Railsback L. (2005) Biomass effects on stalagmite growth and isotope ratios: a 20th century analogue from Wiltshire, England. *Earth Planet. Sci. Lett.* **240**, 486–494.

Baldini J. U. L., McDermott F. and Fairchild I. J. (2006) Spatial variability in cave drip water hydrochemistry: implications for stalagmite paleoclimate records. *Chem. Geol.* **235**, 390–404.

Baldini J. U. L., McDermott F., Hoffman D. L., Richards D. A. and Clipson N. (2008) Very high frequency and seasonal cave atmosphere PCO_2 variability: implications for stalagmite growth and oxygen isotope-based paleoclimate records. *Earth Planet. Sci. Lett.* **272**(1–2), 118–129.

Bao H. M., Fairchild I. J., Wynn P. M. and Spötl C. (2009) Stretching the envelope of past surface environments: neoproterozoic glacial lakes from Svalbard. *Science* **323**(5910), 119–122.

Bao H. M., Lyons J. R. and Zhou C. (2008) Triple oxygen isotope evidence for elevated CO_2 levels after a Neoproterozoic glaciation. *Nature* **453**, 504–506.

Benn D. I., Le Hir G., Bao H., Donnadieu Y., Dumas C., Fleming E. J., Hambrey M. J., McMillan E. A., Petronis M. S., Ramstein G., Stevenson C. T. E., Wynn P. M. and Fairchild I. J. (2015) Orbitally forced ice sheet fluctuations in snowball earth. *Nat. Geosci.* **8**, 704–707.

Borsato A., Frisia S., Fairchild I. J., Somogyi A. and Susini J. (2007) Trace element distribution in annual stalagmite laminae mapped by micrometer resolution X-ray fluorescence: implications for incorporation of environmentally significant species. *Geochim. Cosmochim. Acta* **71**, 1494–1512.

Borsato A., Frisia S., Wynn P., Fairchild I. J. and Miorandi R. (2015) Sulphate concentration in cave drip water and speleothems: long-term trends and overview of its significance as proxy of environmental processes and climate forcing. *Quat. Sci. Rev.* **127**, 48–60.

Borsato A., Johnston V., Frisia S., Miorandi R. and Corradini F. (2016) Temperature and altitudinal influence on karst drip water chemistry: implications for regional-scale paleoclimate reconstructions from speleothems. *Geochim. Cosmochim. Acta* **177**, 275–297.

Bottrell S. H. and Newton R. J. (2006) Reconstruction of changes in global sulphur cycling from marine sulphate isotopes. *Earth Sci. Rev.* **75**, 59–83.

Burdett J. W., Arthur M. A. and Richardson M. (1989) A Neogene seawater isotope age curve from calcareous pelagic microfossils. *Earth Planet. Sci. Lett.* **94**, 189–198.

Busenberg E. and Plummer L. N. (1985) Kinetic and thermodynamic factors controlling the distribution of SO_4^{2-} and Na^+ in calcites and selected aragonites. *Geochim. Cosmochim. Acta* **49**, 713–725.

Day C. and Henderson G. M. (2013) Controls on trace-element partitioning in cave-analogue calcite. *Geochim. Cosmochim. Acta* **120**, 612–627.

Fairchild I. J., Borsato A., Tooth A., Frisia S., Hawkesworth C. J., Huang Y., McDermott F. and Spiro B. (2000) Controls on trace element (Mg-Sr) compositions of carbonate cave waters: implications for speleothem climatic records. *Chem. Geol.* **166**, 255–269.

Fairchild I. J., Tuckwell G. W., Baker A. and Tooth A. F. (2006) Modelling of drip water hydrology and hydrogeochemistry in a weakly karstified aquifer (Bath, UK): implications for climate change studies. *J. Hydrol.* **321**, 213–231.

Fairchild I. J., Spötl C., Frisia S., Borsato A., Susini J., Wynn P. M., Cauzid J. and EIMF (2010) Petrology and geochemistry of annually laminated stalagmites from an Alpine cave (Obir, Austria): seasonal cave physiology. In *Tufas and Speleothems: Unravelling the Microbial and Physical Controls* (eds. H. M. Pedley and M. Rogerson). Geol. Soc. Lond. Spec. Publ., 336, pp. 295–321.

Fairchild I. J. and Baker A. (2012) *Speleothem Science. From Process to Past Environment*. Wiley, Chichester.

Feng J., Lee Y. J., Reeder R. J. and Phillips B. L. (2006) Observation of bicarbonate in calcite by NMR spectroscopy. *Am. Mineral.* **91**, 957–960.

Frisia S., Borsato A., Fairchild I. J. and McDermott F. (2000) Calcite fabrics, growth mechanisms, and environments of formation in speleothems from the Italian alps and southwestern Ireland. *J. Sediment. Res.* **70**(5), 1183–1196.

Frisia S., Borsato A., Fairchild I. J. and Susini J. (2005) Variations in atmospheric sulphate recorded in stalagmites by synchrotron micro XRF and XANES analyses. *Earth Plan. Sci. Lett.* **235**, 729–740.

Frisia S., Borsato A. and Susini J. (2008) Synchrotron radiation applications to past volcanism archived in speleothems: an overview. *J. Volcanol. Geotherm. Res.* **177**, 96–100.

Frisia S., Fairchild I. J., Fohlmeister J., Miorandi R., Spötl C. and Borsato A. (2011) Carbon mass-balance modelling and carbon isotope exchange processes in dynamic caves. *Geochim. Cosmochim. Acta* **75**, 380–400.

Fuller L. (2006) High-resolution multiproxy geochemical Holocene climate records from 1000-year old Scottish Stalagmites. Ph.D. Thesis, University of Birmingham.

Fuller L., Baker A., Fairchild I. J., Spötl C., Marca-Bell A., Rowe P. and Dennis P. F. (2008) Isotope hydrology of dripwaters in a Scottish cave and implications for stalagmite paleoclimate research. *Hydrol. Earth Syst. Sci.* **12**(4), 1065–1074.

Hartland A., Fairchild I. J., Lead J. R., Zhang H. and Baalousha M. (2011) Size, speciation and lability of NOM-metal complexes in hyperalkaline cave drip water. *Geochim. Cosmochim. Acta* **75**, 7531–7577.

Hartland A., Fairchild I. J., Lead J. R., Borsato A., Baker A., Frisia S. and Baalousha M. (2012) From soil to cave: transport of trace metals by natural organic matter in karst drip waters. *Chem. Geol.* **304**, 68–82.

Huang Y. and Fairchild I. J. (2001) Partitioning of Sr^{2+} and Mg^{2+} into calcite under karst-analogue experimental conditions. *Geochim. Cosmochim. Acta* **65**, 47–62.

Hughes S. G., Taylor E. L., Wentzell P. D., McCurdy R. F. and Boss R. K. (1994) Models of conductance measurement in quality assurance of water analysis. *Anal. Chem.* **66**, 830–835.

James E. W., Banner J. L. and Hardt B. (2015) A global model for cave ventilation and seasonal bias in speleothem paleoclimate records. *Geochem. Geophys. Geosyst.* **16**, 1044–1051.

Leito I., Strauss L., Koort E. and Pihl V. (2002) Estimation of uncertainty in routine pH measurement. *Accred. Qual. Assur.* **7**, 242–249.

Lorens R. B. (1981) Sr, Cd, Mn and Co distribution coefficients in calcite as a function of calcite precipitation rate. *Geochim. Cosmochim. Acta* **45**, 553–561.

McDermott F., Frisia S., Huang Y. M., Longinelli A., Spiro B., Heaton T. H. E., Hawkesworth C. J., Borsato A., Keppens E., Fairchild I. J., van der Borg K., Verheyden S. and Selmo E. (1999) Holocene climate variability in Europe: evidence from delta O-18, textural and extension-rate variations in three speleothems. *Quat. Sci. Rev.* **18**, 1021–1038.

McIntyre W. L. (1963) Trace element partition coefficients – a review of theory and applications to geology. *Geochim. Cosmochim. Acta* **27**, 1029–1264.

Miorandi R., Borsato A., Frisia S., Fairchild I. J. and Richter D. K. (2010) Epikarst hydrology and implications for stalagmite capture of climate changes at Grotta di Ernesto (N.E. Italy): results from long-term monitoring. *Hydrol. Proc.* **24**, 3101–3114.

Mucci A. and Morse J. W. (1983) The incorporation of Mg^{2+} and Sr^{2+} into calcite overgrowths – influences of growth rate and solution composition. *Geochim. Cosmochim. Acta* **47**(2), 217–233.

Nagra G., Treble P. C., Anderson M. S., Fairchild I. J., Coleborn K. and Baker A. (2016) A post-wildfire response in cave dripwater chemistry. *Hydrol. Earth Syst. Sci.* **20**, 2745–2758.

Pingitore N. E. and Eastman M. P. (1986) The co-precipitation of Sr^{2+} with calcite at 25 and 1 atm. *Geochim. Cosmochim. Acta* **50**, 2195–2203.

Pingitore N. E., Meitzner G. and Love K. M. (1995) Identification of sulfate in natural carbonates by X-ray absorption spectroscopy. *Geochim. Cosmochim. Acta* **59**, 2477–2483.

Plummer L. N., Parkhurst D. and Kosiur D. R. (1975) MIX2, a computer program for modeling chemical reactions in natural waters. *U.S. Geological Survey, Water Resources Investigations Report* 61, 75p.

Proctor C. J., Baker A., Barnes W. L. and Gilmour M. (2000) A thousand year speleothem proxy record of North Atlantic climate from Scotland. *Clim. Dyn.* **16**, 815–820.

Przybylinski J. L. (1987) The role of bicarbonate ion in calcite scale formation. *Soc. Petrol. Eng.* **2**, 63–67.

Reeder R. J., Lamble G. M., Lee J. F. and Staudt W. J. (1994) Mechanism of SeO_4^{2-} substitution in calcite: an EXAFS study. *Geochim. Cosmochim. Acta* **58**, 5639–5646.

Rennie V. C. F. and Turchyn A. (2014) The preservation of $\delta^{34}S_{SO4}$ and $\delta^{18}O_{SO4}$ in carbonate associated sulfate during marine diagenesis: A 25Myr test case using marine sediments. *Earth Planet. Sci. Lett.* **395**, 13–23.

Rossum J. R. (1975) Checking the accuracy of water analyses through the use of conductivity. *J. Amer. Water Wells Assoc.* **67**, 204–205.

Sherwin C. M. and Baldini J. U. L. (2011) Cave air and hydrological controls on prior calcite precipitation and stalagmite growth rates: implications for paleoclimate reconstructions using speleothems. *Geochim. Cosmochim. Acta* **75**(14), 3915–3929.

Smith C. L., Fairchild I. J., Spötl C., Frisia S., Borsato A., Moreton S. G. and Wynn P. M. (2009) Chronology-building using objective identification of annual signals in trace element profiles of stalagmites. *Quat. Geochron.* **4**, 11–21.

Spötl C., Fairchild I. and Tooth A. F. (2005) Cave air control on drip water geochemistry, Obir Caves (Austria): implications for speleothem deposition in dynamically ventilated caves. *Geochim. Cosmochim. Acta* **69**, 2451–2468.

Staudt W. J., Reeder R. and Schoonen M. A. (1994) Surface structural controls on compositional zoning of SO_4^{2-} and SeO_4^{2-} in synthetic calcite single crystals. *Geochim. Cosmochim. Acta* **58**(9), 2087–2098.

Tooth A. F. and Fairchild I. J. (2003) Soil and karst aquifer hydrological controls on the geochemical evolution of speleothem forming drip waters, Crag Cave, southwest Ireland. *J. Hydrol.* **273**, 51–68.

Treble P. C., Fairchild I. J., Baker A., Meredith K. T., Anderson M. S., Salmon S. U., Bradely C., Wynn P. M., Hankin S., Wood A. and McGuire E. (2016) Roles of forest bioproductivity, transpiration, and fire in a nine-year record of cave dripwater chemistry from southwest Australia. *Geochim. Cosmochim. Acta* **184**, 132–150.

Uchida S., Kurisaki K., Ishihara Y., Haraguchi S., Yamanaka T., Noto M. and Yoshimura K. (2013) Anthropogenic impact records of nature for past hundred years extracted from stalagmites in caves found in the Nanatsugama Sandstone Formation, Saikai, Southwestern Japan. *Chem. Geol.* **347**, 59–68.

Uchikawa J., Harper D. T., Penman D. E., Zachos J. C. and Zeebe R. E. (2017) Influence of solution chemistry on the boron content in inorganic calcite grown in artificial sweater. *Geochim. Cosmochim. Acta* **218**, 291–307.

van der Weijden R. D., van der Heijden R. D., Witkamp G. J. and van Rosmalen G. M. (1997) The influence of total calcium and total carbonate on the growth rate of calcite. *J. Cryst. Growth* **171**, 190–196.

van der Weijden C. H. and van der Weijden R. D. (2014) Calcite growth: rate dependence on saturation, on ratios of dissolved calcium and (bi)carbonate and on their complexes. *J. Cryst. Growth* **394**, 137–144.

Wynn P. M., Fairchild I. J., Baker A., Baldini J. U. L. and McDermott F. (2008) Isotopic archives of sulphate in speleothems. *Geochim. Cosmochim. Acta* **72**, 2465–2477.

Wynn P. M., Fairchild I. J., Frisia S., Spötl C., Baker A., Borsato A. and EIMF (2010) High-resolution sulphur isotope analysis of speleothem carbonate by secondary ionization mass spectrometry. *Chem. Geol.* **271**, 101–107.

Wynn P. M., Borsato A., Baker A., Frisia S., Miorandi R. and Fairchild I. J. (2013) Biogeochemical cycling of sulphur in karst and transfer into speleothem archives at Grotta di Ernesto, Italy. *Biogeochemistry* **114**, 255–267.

Wynn P. M., Fairchild I. J., Spötl C., Hartland A., Mattey D., Fayard B. and Cotte M. (2014) Synchrotron X-ray distinction of seasonal hydrological and temperature patterns in speleothem carbonate. *Environ. Chem* **11**, 28–36.

Associate editor: Robert H. Byrne